4-3.Strain accommodation process in a sheared quartz aggregates

Strain accommodation process in a sheared quartz aggregate

Osamu Nishikawa

Department of Earth Science, Faculty of Science, Kanazawa University, Kakuma Kanazawa 920-1192 Japan

Abstract

Strain accommodation process has been investigated using TEM and SEM-EBSP system for a sheared quartz aggregate deformed under higher greenschist facies condition collected from the Hatagawa mylonite zone, Abukuma Mountains in northeast Japan. Microstructural features indicate pervasive operation of both subgrain rotation and grain boundary migration. Dislocation densities and spacings of subgrain boundaries are similar in magnitude (10^8 cm^{-2} orders and 6 μm, respectively), in differently oriented grains. However the grains favorably oriented for operation of $\{10\bar{1}1\}<11\bar{2}0>$ and $\{10\bar{1}0\}<11\bar{2}0>$ slip systems tend to have small mean intra-granular misorientations (less than 3°) and occupy a large volume in the aggregate, while grains favorably oriented for $(0001)<11\bar{2}0>$ slip show large intra-granular misorientations, often exceeding 10°, and seem to have decreased their volume fraction. The subgrain boundary energies of the latter grains are estimated about 0.28 J/m^2, and are 1.5 - 2 times larger than the former. This large gradient of subgrain boundary energy between differently orientated grains could drive a grain boundary migration process.

Key Words : Quartzite, Strain, Dynamic recrystallization, Dislocation, Subgrain.

INTRODUCTION

Deformation of the Earth's crust at metamorphic conditions mostly occurs by crystalline plasticity, which involves movement and multiplication of dislocations in

grains. Strain stored in grains associated with deformation controls deformation behavior of rocks and minerals through strain hardening and following dynamic recrystallization process.

The driving force of dynamic recrystallization is thought to be a gradient of strain energy across boundaries (e.g., Bocher and Jonas 1999). Strain free grains preferentially grow at the expense of highly strained grains, which changes microstructures and average crystallographic orientations rapidly in a steady state. Therefore, the strain accommodation process and grain growth are essential in dynamic recrystallization. The magnitude of strain energy stored in a grain depends on the configuration of dislocations (e.g., Humphreys and Hatherly 1995; Hughes 1999). Pile-up of dislocations, which typically develop in low temperature deformation, generates the highest magnitude of strain energy. On the other hand, under conditions where subgrain rotation process effectively operates, dislocations are rearranged into subgrain boundaries resulting in reduction of bulk strain energy and simultaneously in a heterogeneous energy distribution in a grain. Under such conditions not only single dislocations, but also subgrain boundaries contribute to the stored strain energy (e.g., Jones 1978; Humphreys and Hatherly 1995; Doherty 1997). In deformation experiments of metals up to several ten percents of strain, it has been reported that mean misorientation and spacing of subgrain boundaries depend on the amount of imposed strain and crystallographic orientation (e.g., Bailey and Hirsch 1962; Dillamore et al. 1972; Doherty 1974; Sakai and Ohashi 1990). However, there are few studies that investigate the strain accommodation process in deformed rocks and minerals.

The aim of this paper is to make clear the strain accommodation process in deformed rocks under conditions where both subgrain rotation and grain boundary migration pervasively operate, which is prevailing in widespread metamorphic conditions. Degree and spatial distribution of strain stored in grains and their orientation dependence in sheared quartz aggregates were investigated by observations of dislocation substractures and texture analyses using a TEM and SEM-EBSP system.

SAMPLE DESCRIPTION

A mylonite sample was collected from an outcrop of granodiolite along Uketo-gawa river in the Hatagawa shear zone, trending NNW-SSE in the eastern margin of the Abukuma Mountains, NE Japan (Fig. 1). The age of intrusion of granotoids, exposed in the shear zone, is thought to be Cretaceous. Field evidences revealed that the Hatagawa shear zone had been already active before the intrusion events ceased (e.g., Kubo et al. 1990).

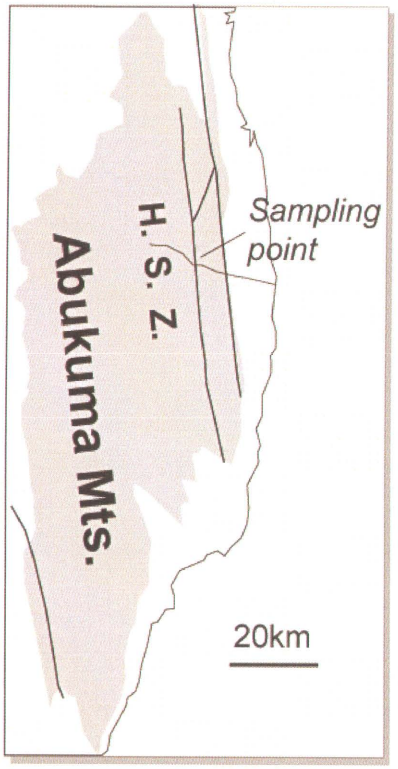

Fig. 1 Map showing sample locality, H. S. Z.: Hatagawa Shear Zone. Shaded area denotes the area Pre-Tertiary rocks exposed.

Fig. 2 Optical micrograph (crossed polarizers) showing the representative microstructures of the studied quartz aggregates in a mylonite collected from Hatagawa shear zone.

In the rocks around the sampling area, steeply dipping mylonitic foliations and stretching lineations parallel to the trend of the shear zone are developed. An orthogonal sample coordinate system has been defined such that X is parallel to the stretching lineation, Z is normal to the foliation plane, and Y is normal to the lineation and parallel to the foliation plane. All the observations were carried out on XZ thin

sections. Clusters of quartz grains are flattened into 1 - 3 mm thick and 10 - 20 mm wide regions. These clusters are often connected forming penetrative networks of quartz aggregates. Analyzed quartzite consists of coarse ribbon and small equant grains (Fig. 2). Ribbon grains, whose mean diameters and aspect ratios are 495 μm and 8.7 respectively, are oriented with their long axes parallel to *X*, forming banding structures. Fine equant grains with 11.1 μm mean diameter and 2.1 mean aspect ratio tend to prevail in highly strained portions, and seem to be recrystallized from ribbon grains. Asymmetric microstructures indicate a sinistral sense of shear. Judging from the similarity of the microstructures of present sample with those described by Stipp et al. (1999) for a subgrain rotation regime, the studied sample probably deformed under middle to higher greenschist facies condition.

ANALYTICAL PROCEDURES

Microstructural observation and TEM measurement of crystallographic orientation

Observation of dislocation substructures and measurement of misorientations across subgrain boundaries were performed with a transmission electron microscope (TEM) using an accelerating voltage of 120 kV and a double tilt specimen holder. The observations were carried out under two-beam conditions. The Burgers vectors of dislocations were determined using the invisibility criteria (e.g., McLaren 1991). For misorientation analysis, crystallographic orientations were determined by TEM in the following way. By tilting the specimen, a low index lattice plane like (0001), $\{11\bar{2}0\}$ or $\{10\bar{1}0\}$ is brought normal to the beam direction to obtain a hexagonal or orthogonal diffraction pattern. The crystallographic orientation can be uniquely determined analyzing the diffraction pattern recorded on the film and reading rotation angles of the specimen holder. The accuracy of measurement for this method is 2 - 3°. The misorientation between two measurement points is expressed by a misorientation matrix **M,** which is related to the orientation matrices for both points **A** and **B** as **AM=B**. The misorientation angle θcan be calculated by using the following relation: $tr\mathbf{M}=1+2\cos\theta$, where *tr* is the trace of the matrix. The rotation axis of the misorientation can be obtained by calculating the Eigen-vector of **M** when the

Eigen-value equals 1. For the subgrain boundaries with very small misorientation (2°>), the misorientation angles were determined by the method of Mawer and Fitz Gerald (1993). Diffraction patterns from both sides of a boundary were recorded simultaneously on a single photograph under the condition that a low index plane of one side was oriented exactly normal to the beam direction. Analyzed quartz crystals were effectively treated as hexagonal in this method, because trigonality could not be identified with TEM diffraction intensities in this orientation.

Crystallographic orientation measurement using SEM-EBSP system

For the crystallographic orientation measurement, a electron back scatter pattern (SEM-EBSP) system was also used. Kikuchi pattern, which is result of electron backscatter diffraction occurred in a very thin layer (< 50 nm) in the polished surface, are crystallographically indexed in this method. The intervals of measurement points were 0.05-0.1 mm in *X* and 0.01 mm in *Z* directions. The crystallographic orientation of each diffraction image was determined by the CHANNEL+ software, produced by HKL Technology. Simulated and observed Kikuchi bands were compared in manual mode in order to confirm the correctness of indexing, particularly with respect to the hexagonal pseudo-symmetry of trigonal α-quartz. The error of the measurement is generally about 1°.

RESULTS

Pole figures of *c* and *a*-axes orientations for the present quartz aggregates are shown in Fig. 3. It mainly consists of two orientation components (Fig. 3): the grains favorably oriented for slip on prism $\{10\bar{1}0\}$ or rhomb $\{10\bar{1}1\}$ plane in $<11\bar{2}0>$ (<*a*>) direction (B-grains) and those favorably oriented for basal (0001)<*a*> slip (W-grains), assuming simple shear on the foliation plane in the lineation direction. A remarkable feature of this pole figure is the fairly strong cross girdle component (B-grains) and relatively weak small circle components (W-grains): an intermediate feature between those typically developed under greenschist facies and amphibolite facies. In optical microscopy, W-grains often isolated as thin layers and equant small grains between ribbon B-grains (Fig. 2). Therefore it can be interpreted that the present sample

represents a transient microstructures in modifying original microstructures developed under the greenshcist facies condition by those of the lower amphibolite facies condition. This may be associated with the change of dominantly activated slip systems from basal<*a*> to rhomb<*a*> and prism<*a*>.

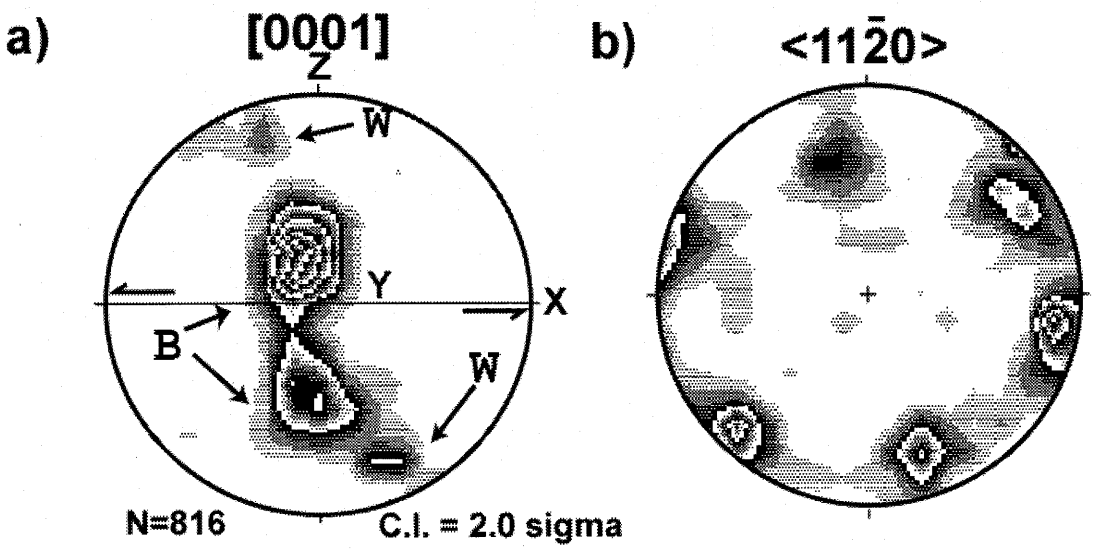

Fig. 3 Pole figures of crystallographic orientations for studied quartz aggregates, measured by a SEM-EBSP system (816 grains). Lower hemisphere, equal area projection. a) *c*[0001]. B and W denote the orientation components of the B- and W-grains, respectively, b) *a*<11$\bar{2}$0>.

TEM microscopy revealed that many dislocations and subgrain boundaries are pervasively developed in a whole grain (Fig. 4a). Most of dislocations are approximately parallel to rhomb and prism planes, and dislocations parallel to basal plane also observed in W-grains (Table 1, Fig. 4b). In two beam condition, almost all dislocations are in strong contrast for the reflection g=1011, and have zero or very weak contrast for the reflection g= 0003, consistent with a Burgers vector b=<*a*> (Fig. 4c, d). Therefore, rhomb and prism<*a*> are suggested as dominant slip systems, and basal<*a*> slip system seems to have also operated in W-grains. This observation is consistent with the inference from the LPO patterns (Fig. 3). Mean free dislocation densities in the present sample are generally ranging from 3.1 to 7.8×10^{8} cm^{-2}, and no significant differences exceeding heterogeneities observed in a single grain are found among differently oriented grains (Table 1).

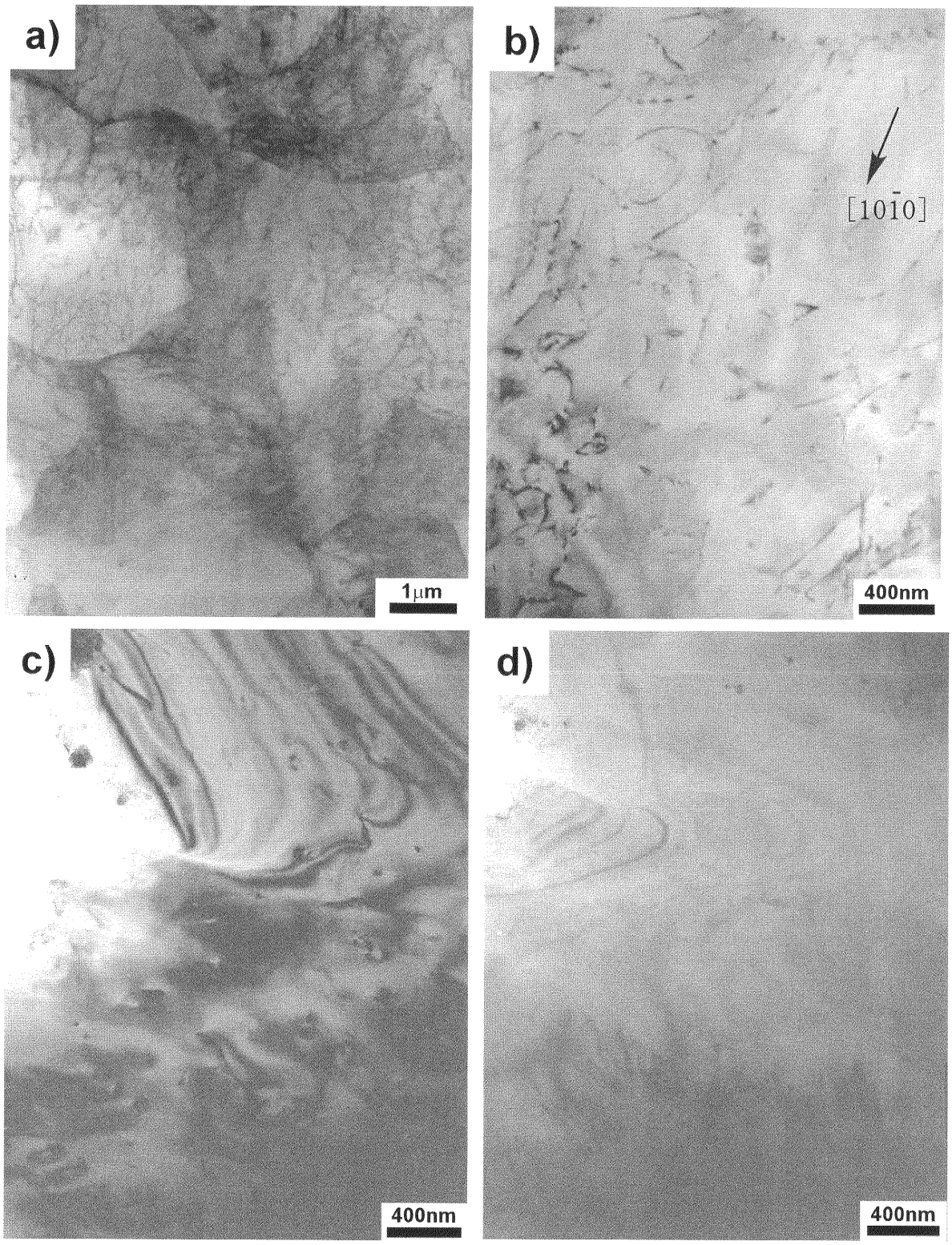

Fig. 4 TEM bright field images of dislocation substructures developed in grains.

a) Dislocations and subgrains pervasively developed, b) Many dislocations array about 52° oblique and parallel to the prism (10$\bar{1}$0) plane, c) Dislocations are in strong contrast for the reflection g=10$\bar{1}$0, d) Most of dislocations are out of contrast for g=0003.

The spacing of subgrain boundaries and their misorientations were measured along transects in grains (Fig. 5). Although subgrain boundaries are similarly spaced, approximately 5.7 μm in W-grains and 5.8 μm in B-grains, misorientations of subgrain boundaries show significant orientation dependence of the host grain. The subgrain boundaries in B-grains generally have small misorientations (< 3°, Fig. 5a). On the other hand, those in W-grains often include subgrain boundaries with larger misorientations (Fig. 5b).

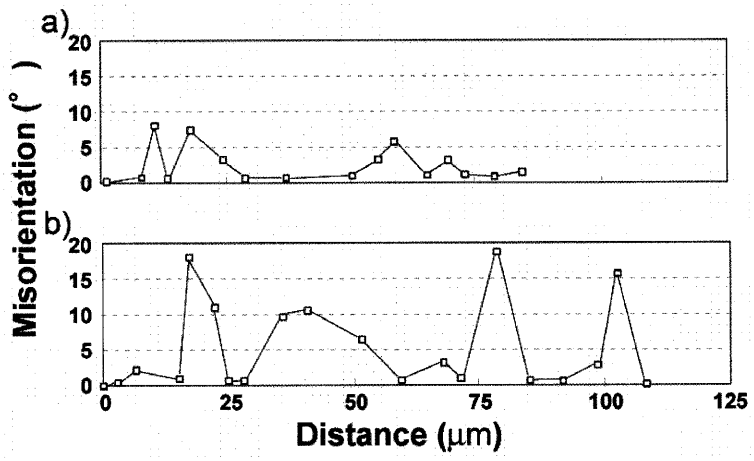

Fig. 5 Misorientations and spacings of subgrain boundaries along transects. a) a B-grain, b) a W-grain.

Misorientations between neighboring measurement points of EBSP were calculated for ribbon grains. In order to investigate the relation between magnitude of intra-granular misorientations and bulk crystallographic orientations of the grains, the mean intra-granular misorientations have been investigated as a function of the Schmid factor of the grain. When several potential slip systems with the same critical resolved shear stress are available, the relative ease of slip on a certain slip system can be quantitatively expressed by the Schmid factor (*Sss*; Law et al. 1990). In Fig. 6, the mean intra-granular misorientations of differently oriented grains are plotted as a function of *Sss* for the prism<*a*> slip system. *Sss* of B-grains are generally higher than 0.75 meaning favorably oriented for opperation of prism<*a*> slip systems, while W-grains are clustered around *Sss* value less than 0.55. Although no clear systematic changes are found among each *Sss* cluster, there is a distinct gap of magnitude of misorientation between these *Sss* clusters. The mean misorientations in the B-grains are very low, ranging from 1° to 4°, while misorientations in the W-grains are spatially inhomogeneous and mostly around 10°, with large standard deviations.

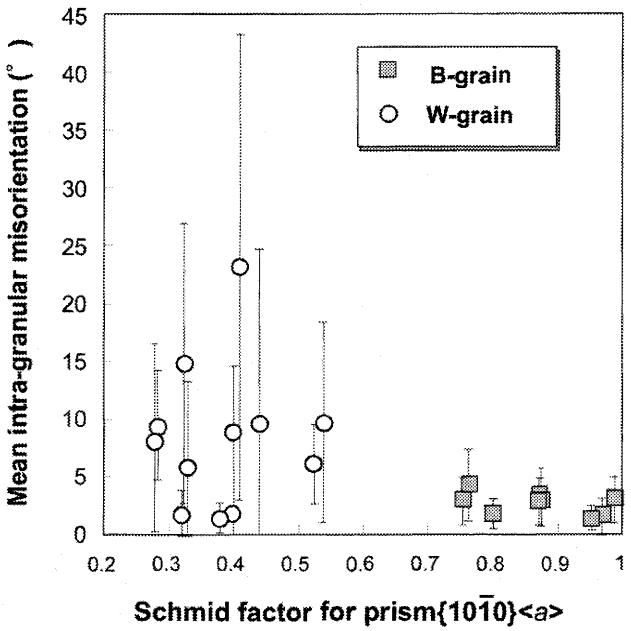

Fig. 6 Mean intra-gramular misorientations for differently oriented grains plotted as a function of the Schmid factor for prism <*a*>

Table 1 Dislocation densities and distribution patterns on the photomicrographs of TEM.
W: W-grain which is favorably oriented for (0001)<11$\bar{2}$0> (basal<*a*>) slip, B: B-grain which is favorably oriented for prism{10$\bar{1}$0}<*a*> and rhomb{10$\bar{1}$1}<*a*> slips

Samples	Grains	Dislocation density (cm^{-2})	Distribution pattern of dislocations
Qz-s4-1	W	$7.3x10^8$	Dominantly parallel to {10$\bar{1}$1}, Subparallel to (0001)
Qz-s4-3	W	$6.1x10^8$	Dominantly parallel to {10$\bar{1}$1}, subordinately {10$\bar{1}$0}
Qz-s4-5	B	$4.5x10^8$	Apparently random distribution
Qz-s4-7	B	$3.1x10^8$	Parallel to {10$\bar{1}$1} and {10$\bar{1}$0}
Qz-s4-9	B	$6.0x10^8$	Very high angle to (0001)
Qz-s4-10	B	$7.2x10^8$	Very high angle to (0001)
Qz-s4-11	B	$4.0x10^8$	Mostly parallel to {10$\bar{1}$1}
Qz-s4-13	W	$3.8x10^8$	Apparently random distribution
Qz-s4-14	B	$4.7x10^8$	Both high and low angle to (0001)
Qz-s4-15	W	$7.8x10^8$	Dominantly parallel to {10$\bar{1}$1}, subordinately (0001)
Qz-s4-17	B	$6.9x10^8$	Mostly parallel to {10$\bar{1}$1}

DISCUSSION AND CONCLUSIONS

It is reasonable to consider that the nuclei of new grains were originally strain free, and therefore they could grow rapidly, consuming more highly deformed old grains. However, since they deform as they grow, the growth rate would decrease with increase of dislocations in the new grains. It has been shown experimentally that the free dislocation density saturates quickly in an early stage of deformation under conditions where recovery process effectively operates. Kirby and McCormick (1979) reported that the dislocation density in quartz becomes independent of strain after only a few percent of deformation. Consequently the difference in dislocation density between new and old grains would be reduced. After dislocations multiplied to a critical density, excess dislocations would annihilate each other or form subgrain boundaries. It has been also known that the spacing of subgrain boundaries shows a strain dependence during early stage of deformation and reach a steady state after an initial rapid development. Sakai and Ohashi (1990) demonstrated for hot-deformed nickel that the subgrain size reached a steady state at about 50 % of the peak stress strain, which corresponds to about 10 % of imposed strain. Karato et al. (1980) showed in a high-temperature experiment of olivine single crystals that the dislocation density reached first a steady state, and followed by subgrain formation, before dynamic recrystallization occurred. In the present sample, dislocation densities and subgrain boundary spacings are of the same order of magnitude in B and W-grains (10^8 cm^{-2} orders and 6 μm, respectively). Therefore, it can be considered that dislocation densities and subgrain boundary spacings of most of the grains had already reached steady state, and, with further deformation, they would only be subject to an increase of misorientation of subgrain boundaries. In fact, only the mean intra-granular misorientations are notably different: generally higher than 10° in W-grains and less than 3° in B-grains.

Here let's will evaluate the difference of subgrain boundary energy between W- and B-grains. Read and Shockley (1950) estimated the grain boundary energy E of symmetric low angle tilt boundary per unit area as:

$$E=\mu b/4\pi(1-\nu)\cdot\theta(A_0-\ln\theta) \quad (1)$$

where θ is the misorientation angle, μ and ν are shear modulus and Poison's ratio, respectively. A_0 is a term related to the dislocation core energy:

$$A_0=1+\ln(b/r_0)+4\pi(1-\nu)/\mu b^2\cdot E_0 \quad (2)$$

where r_0 is the radius of the dislocation core, E_0 is the core energy. Equation (1) describes that the boundary energy increases with the higher misorientation angle θ. Using equation (1) with the values: $|b| = d(1120) = 4.9$ Å, $r_0 = b$ (e.g., Poirier 1985; Wintsch and Dunning 1985), μ=43.6 GPa and ν=0.026 (for 386 °C; Ohno 1995) and neglecting the unknown term for the core energy in equation (2), the mean subgrain boundary energies E are estimated to be 0.279 J/m^2 for W-grains and 0.15 - 0.2 J/m^2 for B-grains. The estimated subgrain boundary energy in the W-grains is about 1.5 - 2 times larger than in B-grains.

Microstructural features in the present sample described above indicate that grains favorably oriented for operation of prism<*a*> and rhomb<*a*> slip systems grew at the expense of those for basal<*a*> slip. It could be concluded that the driving force of grain boundary migration was provided by this large gradient of subgrain boundary energies between these differently oriented grains.

ACKNOWLEDGEMENT

I would like to thank Rudy Wenk, Yanxia Xie, John Donovan and Timothy Teague for their helps with the EBSP measurements in UC Berkeley. I am grateful to Jun-Ichi Ando for arranging TEM experiments at Hiroshima University.

REFERENCES

Bailey, J. E. and Hirsch, R. B. (1962) The recrystallization process in some polycrystalline metals. *Proceedings of the Royal Society* **A267**, 11-30.

Bocher, Ph. and Jonas, J. J. (1999) Characteristics of nucleation and grouth during the dynamic recrystallization of a 304 strainless steel. In: Sakai, T., and Suzuki, H. G.,

(Eds.), Proceedings of ReX'99, The 4th International Conference on Recrystallization and Related Phenomina, pp. 25-36.

Dillamore, I. L., Morris, P. L., Smith, C. J. E. and Hutchinson, W. B. (1972) Transition bands and recrystallization in metals. *Proceedings of Royal Society of London* A. **329**, 405-420.

Doherty, R. D. (1997) Recrystallization and texture. *Progress in Material Science* **42**, 39-58.

Herwegh, M. and Handy, M. R. (1996) The evolution high-temperature mylonitic microfabric: evidence from simple shearing of a quartz analogue (norcamphor). *Journal of Structural Geology* **18**, 689-710.

Hughes, D. A. (1999) Dislocations of low and high angle boundaries in deformed metals. In: Sakai, T., and Suzuki, H. G., (Eds.), Proceedings of ReX'99, The 4th International Conference on Recrystallization and Related Phenomina, pp. 111-118.

Humphreys, F. J. and Hatherly, M. (1995) Recrystallization and Related Annealing Phenomena, Pergamon, Oxford, pp. 520.

Jones, A. R. (1978) Grain boundary phenomena during the nucleation of recrystallization, In F. Haessener, Dr. Rieder Verlag, Stuttgart (Eds), Recrystallization of Metallic Materials, 379-425.

Karato, S. I., Toriumi, M. and Fujii, T. (1980) Dynamic recrystallization of olivine single crystals during high-temperature creep. *Geophysical Research Letter* **7**, 649-652.

Kirby, S. H. and McCormick, J. W. (1979) Creep of hydrolytically weakened synthetic quartz crystals oriented to promote {2110}<0001> slip: a brief summary of work to date. *Bull. Mineral.* **120**, 124-137.

Kubo, K., Yanagisawa, Y., Yoshioka, T., Yamamoto, T. and Takizawa, F. (1990) Geology of the Haramachi and Omika district. With Geological Sheet Map at 1: 50,000, Geol. Surv. Japan (in Japanese with English abstruct).

Law, R. D., Schmid, S. M. and Wheeler, J. (1990) Simple shear deformation and quartz crystallographic fabric: a possible natural example from the Torridon area of NW Scotland. *Journal of Structural Geology* **12**, 29-45.

Mawer, C. K. and Fitz-Gerald, J. D. (1993) Microstructure of kink band boundaries in naturally deformed Cewings Range Quartzite. In: Boland, J. N. and Fitz-Gerald, J. D., (Eds.), Defects and Processes in the Solid State: Geoscience Applications The McLaren Volume, pp. 49-67 Elsevier, Amsterdam.

McLaren, A. C. (1991) Transmission Electron Microscpy of Minerals and Rocks, Cambridge University Press, Cambridge, pp. 399.

Ohno, I. (1995) Temperature variation of elastic properties of α-quartz up to the α-β transition. *Journal of Physics of the Earth* **43**, 157-169.

Poirier, J. P. (1985) Creep of Crystals. High-temperature Deformation Processes in Metals, Ceramics and Minerals. Cambridge University press, Cambridge, pp. 260.

Read, W. T. and Shockley, W. (1950) Dislocation models of crystal grain boundaries. *Physical Review* **78**, 275-289.

Sakai, T. and Ohashi, M. (1990) Dislocation substructures developed during dynamic recrystallization in polycrystalline nickel. *Materials Science and Technology* **6**, 1251-1257.

Stipp, M., Stünitz, H. and Heilbronner, R. (1999) Temperature dependence of quartz dynamic recrystallization regimes in naturally deformed rocks. Abstr. Int. Meet. Def. Mech. Rheol. Microstruct. Neustadt, 22 - 26.

Wintsch, P. and Dunning, J. (1985) The effect of dislocation density on the aqueous solubility of quartz and some geologic implications: A theoretical approach. *Journal of Geophysical Research,* **90**, 3649-3657.